




Article

Creep of High-Strength Steel Coated with Plasma Sprayed Self-Fluxing Alloy

Denison A. Moraes ¹, Gisele F. C. Almeida ¹, Antonio A. Couto ¹, Marcos Massi ¹, Felipe R. Caliar ² and Carlos R. C. Lima ^{1,*}

¹ School of Engineering, Mackenzie Presbyterian University, São Paulo 01302-907, Brazil

² Center for Thermal Spray Research, Stony Brook University, 100 Nicolls Rd, Stony Brook, NY 11794, USA

* Correspondence: carlos.lima@mackenzie.br; Tel.: +55-19-99766-2900

Abstract: This article compares the creep testing behavior of AISI 4340 high-strength steel in the as-received and coated conditions. The coating material used was a NiCrBSi self-fluxing alloy. The microstructural characterization was carried out using optical and scanning electron microscopy. The creep tests were conducted at a temperature of 550 °C and with loads of 200, 250, and 300 MPa. The microstructure analysis of the deposited layer revealed some inclusions, very low porosity, and good adhesion to the substrate. The results of the creep tests indicated a decrease in the time to rupture under loads of 250 and 300 MPa for the coated steel. At a load of 200 MPa, the coated steel presented longer times to rupture and higher yield strength, demonstrating an improvement over the uncoated steel under these test condition. The fracture surface inspection showed a failure by a ductile fracture in both samples, with and without coating.

Keywords: AISI 4340 steel; plasma spray; creep; self-fluxing alloy



Citation: Moraes, D.A.; Almeida, G.F.C.; Couto, A.A.; Massi, M.; Caliar, F.R.; Lima, C.R.C. Creep of High-Strength Steel Coated with Plasma Sprayed Self-Fluxing Alloy. *Metals* **2023**, *13*, 763. <https://doi.org/10.3390/met13040763>

Academic Editor: Fang Wang

Received: 4 March 2023

Revised: 8 April 2023

Accepted: 10 April 2023

Published: 14 April 2023



Copyright: © 2023 by the authors. Licensee MDPI, Basel, Switzerland. This article is an open access article distributed under the terms and conditions of the Creative Commons Attribution (CC BY) license (<https://creativecommons.org/licenses/by/4.0/>).

1. Introduction

AISI 4340 steel is classified as ultra-high strength with medium carbon content and low alloying elements. It is widely used in the aeronautical and automobile industries because of its high mechanical resistance, particularly in creep conditions [1]. However, this alloy may be subject to oxidizing environments and mechanical stress at high temperatures. In these situations, a surface treatment has been indicated to maintain a high mechanical resistance [2]. The quenching process is used to harden the alloy by heating it to the austenitizing temperature followed by fast cooling [3,4]. Under creep conditions, grain boundary slip occurs. The grain size of a polycrystalline material results from several manufacturing processes, such as thermal and mechanical treatments. It is generally accepted that the creep rate decreases as the grain size increases [5]. Protective coatings are often applied to steels to enhance their performance under more severe conditions, including wear and corrosion. With a protective coating or a surface modification process, the substrate response to mechanical and thermal solicitations has been found to behave differently [6,7]. The coating may influence mechanical behaviors by changing the stress field at the surface level. Several researchers have studied the impact of coatings on the mechanical properties of materials, but there is still little consensus among them [8–12]. For some authors, depending on the surface treatment process, the deterioration in mechanical properties of the coated alloy results from a decrease in the load-bearing section [8,10]. Others have suggested that the microstructure in the matrix caused by heat treatment is the main factor [9]. Additionally, brittle intermetallic compounds can create vertical and interface cracks under creep stress, contributing to the poorer mechanical properties of the coated materials [11,12]. Therefore, the influence of specific coatings on the properties of the substrate still needs to be clarified.

The influence of coatings or surface modifications on metallic substrates, specifically steels, has been studied. However, there is no full agreement on the benefits of surface

modifications on the creep behavior of the coated samples. Zhang et al. [13] conducted a study on the influence of plasma sprayed NiCr and NiCrAl coatings on the creep resistance of a nickel alloy at 760 °C. They found that the coatings had a beneficial effect on improving the creep resistance of the substrate. The coatings had a final thickness of 300 µm and the creep tests were performed at low stress levels, ranging from 55 to 95 MPa. For all the coated specimens, tertiary creep governed the total creep deformation.

In another study, Zhang et al. [14] assessed the creep behavior of 9Cr-1Mo steel with an MCrAlY coating. The coating was applied by HVOF (High Velocity Oxygen Fuel) spray process at a thickness of 280 µm. The coating had a beneficial effect on the creep resistance of the steel by reducing the cross-sectional stress and preventing oxidation attack on the substrate during creep tests at 550 °C and loads between 197 and 233 MPa. It generally reduced the creep rate and prolonged the onset of tertiary creep, leading to an increase in the creep life.

Xu et al. [15] studied the influence of an aluminide coating deposited on commercial T92 steel by pack cementation. The creep rupture life of the coated and uncoated T92 was investigated, showing that the rupture life of the coated T92 decreased by 46% at the creep stress of 110 MPa and 675 °C compared to the uncoated steel.

Self-fluxing coatings were developed in the 1950s as nickel alloys with the addition of Cr, B, Si, and C [16]. Boron and silicon were added to nickel to improve flux properties, forming borosilicates, which protect against oxidation, and together with chromium, lower the melting temperature of pure nickel, being indicated for protection of the base material to improve its lifetime utility [17]. The Ni-Cr-B-Si coating was studied in working conditions that combined wear, corrosion, and high temperatures [18].

Self-fluxing coatings are applied by several processes, one of which is the widely used atmospheric plasma spray (APS) [19]. The APS technique uses an electric arc as a heat source, generating high temperatures in a plasma jet. It produces high-density coatings and high adhesion to the substrate, with the material applied in powder form. Oxygen from the air can enter the plasma jet, forming oxides, which is characteristic of this coating type [20]. However, this method can lead to irregularly shaped pore, and coatings are subject to the formation of interconnected porosity due to a lack of fusion of sprayed particles or the expansion of gases generated during the deposition process [21]. As a result, self-fluxing coatings often require post-treatment, such as remelting. This can improve adhesion, density, and the presence of pores and interlamellar voids [22].

However, the remelting process can cause residual stresses and cracks in the coating. If there is no reasonable temperature control during remelting, phase transformations may also occur, leading to the appearance of cracks. The remelting process also generates additional costs to the process [23]. In high-temperature applications, premature failure of 4340 steel is associated with creep deformation [24,25]. Therefore, this study aims to analyze the impact of self-fluxing coating applied by air plasma spray on AISI 4340 steel under creep conditions. The results are compared with the original steel substrate.

2. Materials and Methods

The samples were prepared for the creep tests using AISI 4340 steel without heat treatment, as illustrated in Figure 1. The samples were machined in compliance with the ASTM E139-11 specification [26] for creep tests from a commercially available 5/8-inch round bar. The chemical composition of the AISI 4340 steel used in this study meets the ASTM A29/29M standard [27], as shown in Table 1. The melting point of AISI 4340 steel is 1505 °C.

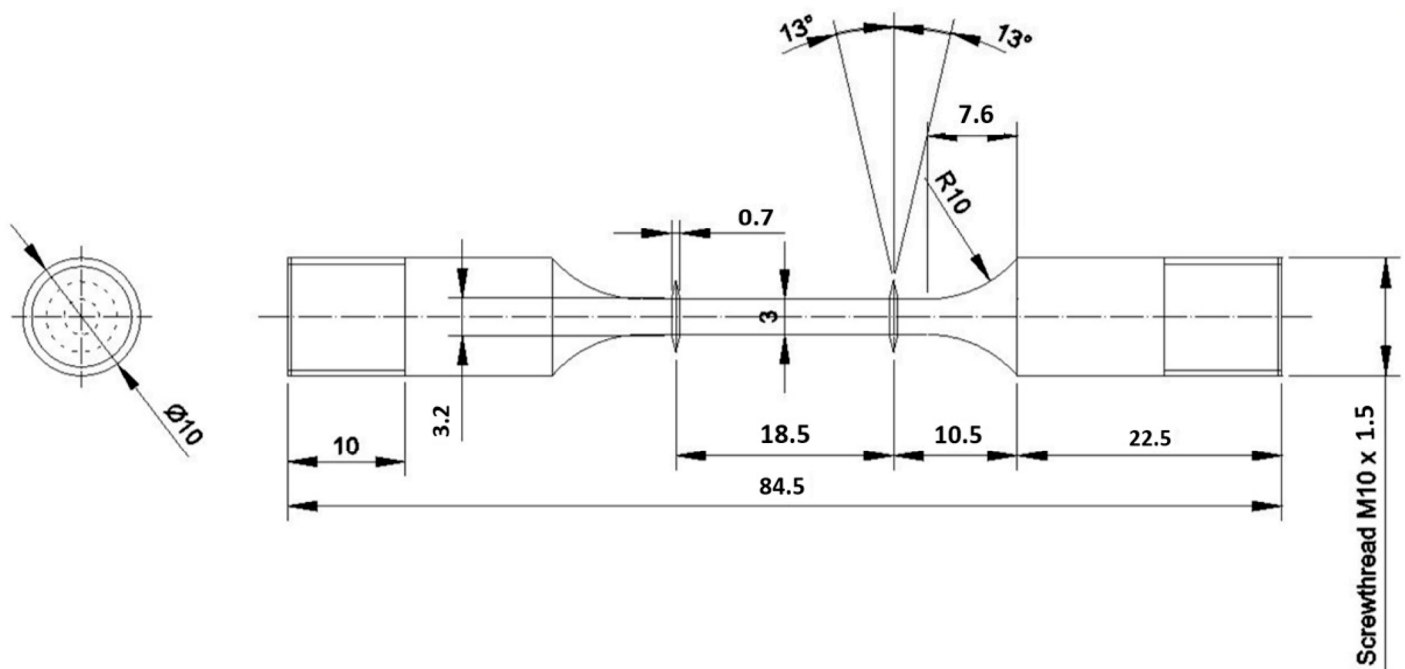


Figure 1. Creep test sample according to ASTM E139-11 (dimensions in mm).

Table 1. Chemical composition of AISI 4340.

| Element | C | Mn | F | S | Si | Ni | Cr | Mo | Fe |
|---------|-----------|---------|-------|------|-----------|----------|---------|---------|------|
| %weight | 0.38–0.43 | 0.6–0.8 | 0.035 | 0.04 | 0.15–0.35 | 1.65–2.0 | 0.7–0.9 | 0.2–0.3 | Bal. |

Diamalloy 2001 alloy (Oerlikon Metco, Westbury, NY, USA) was used as coating material, with spheroidal morphology and particle size distribution ranging from -45 to $+15$ μm . The chemical composition is provided in Table 2. The coating was applied by atmospheric plasma spray (APS) using the parameters outlined in Table 3. The equipment used was the Thermach AT3000, plasma torch SG-100 (Thermach, Appleton, WI, USA), with Mach 1 configuration, coupled with a Staubli 6-axis robot (Staubli, Duncan, Sc, USA).

Table 2. Diamalloy 2001 self-fluxing alloy composition [28].

| Element | Ni | Cr | B | Si | C | Fe |
|----------|---------|----|-----|----|---|----|
| % weight | Balance | 17 | 3.5 | 4 | 1 | 4 |

Table 3. Atmospheric plasma spray parameters.

| Parameters | Value |
|-----------------------|-----------|
| Argon flow rate | 53 L/min |
| Hydrogen flow rate | 1.6 L/min |
| Carrier gas flow rate | 2.8 L/min |
| Powder feed rate | 25 g/min |
| Current | 750 A |
| Standoff Distance | 100 mm |

The samples were grit blasted with Al_2O_3 and then cleaned with deionized water. Immediately before coating deposition, preheating was performed by three passes of the plasma torch at a temperature of 200 $^\circ\text{C}$. Figure 2 depicts a specimen for the creep test, both as it was received and after being coated.



Figure 2. Samples for creep testing (a) as received and (b) coated.

Uniaxial tensile creep tests were conducted using loads of 200, 250, and 300 MPa at a temperature of 550 °C. The Zwick–Roell equipment, model KAPPA 10DS (Zwick–Roell, Ulm, DE), was used for the tests, equipped with a Eurotherm 2604 (Eurotherm, Campinas, SP, Brazil) temperature controller, a transformer linear variable differential (LVDT–Linear Variable Differential Transformer) HBM 1-WA/50MM-T, a Stegmaier-Haupt RX330CR1 servomotor, a split Zwick–Roell furnace, Xforce K load cell (10 kN) and proprietary software “testXpert II” (Zwick–Roell, Campinas, SP, Brazil). One individual sample was tested for creep under each load and coating condition.

Optical microscopy analyses were carried out on a cross-section of coated samples using the Olympus microscope model OM-BX60M (Olympus, Waltham, MA, USA). The samples were prepared by standard metallography procedures involving different sandpapers and subsequent polishing. After the creep test, fractographic analyses of the coated and uncoated samples were performed using a scanning electron microscope (SEM) JEOL JSM-6510 (JEOL, Peabody, MA, USA), coupled to an energy dispersive spectrometer—EDS. Vickers microhardness measurements were taken on the surface of the coated substrate with the Zwick–Roell—EMCO-TEST machine (Zwick–Roell, Ulm, DE).

3. Results and Discussion

3.1. Microstructural Characterization

The applied coating exhibited good adhesion to the substrate and the typical porosity characteristics of such coatings, as shown in Figure 3. It is also possible to observe some porosity in the coating and some oxidation at the coating–substrate interface. This thin layer (around 2–4 µm) is present along almost the entire coating/substrate interface. It might have been present because the sample has gone through the blasting process with Al₂O₃, in addition to sample preheating. Grit blasting induces compressive residual stresses, which depend strongly on the blasted material, blasting material and grit size, blasting time, angle between nozzle, and blasting pressure. Compressive stresses occur below the blasted surface due to plastic deformation of the material, distributed in a very thin layer beneath the surface. The affected zone and the value of the compressive peak increase strongly with grit size, blasting pressure, and blasting time [29]. The subsequent spraying process is more significant in changing the “composite” material (substrate + coating) properties than the blasting process alone [30].

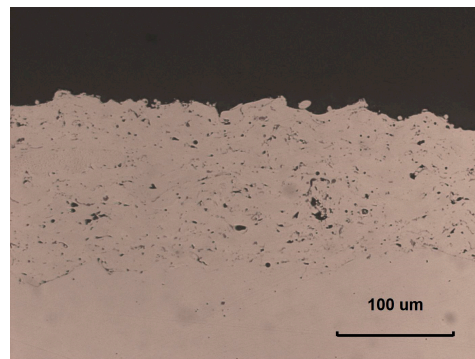


Figure 3. Optical microscopy image of the cross-section of the coating.

Microstructural analyses revealed an average coating thickness of 100 μm, with a tolerance of +15/−10 μm. The microstructure of the substrate as received was also observed by optical microscopy. The substrate did not receive heat treatment, characterized and tested as supplied. After chemical etching using a 2% Nital reagent, the present phases displayed shades of gray. In Figures 4 and 5, it is possible to observe the material's microstructure, before and after coating process, respectively, consisting of a mixture of more resistant phases enriched with carbon (perlite, bainite, and martensite), a typical structure of AISI 4340 steel [31].

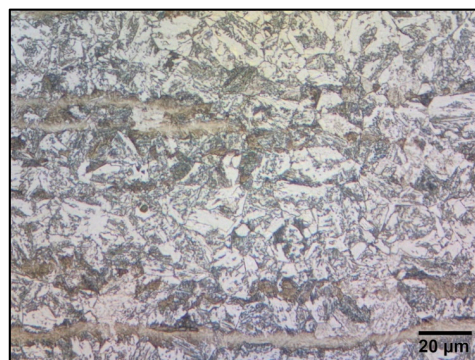


Figure 4. Optical image of AISI 4340 microstructure as received.

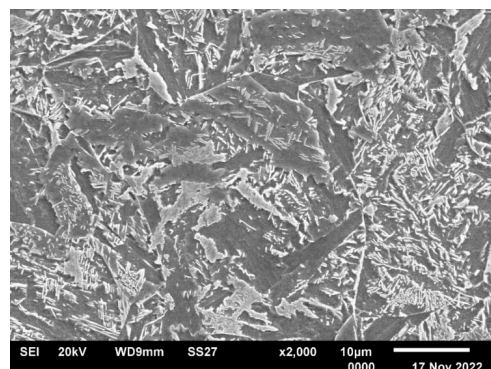


Figure 5. SEM image of the microstructure of AISI 4340 steel after coating process.

The microhardness of the coating was measured at ten different points along the center of the coating thickness, spanning horizontally across the cross-section. The average microhardness was 1116 HV_{0.5}, with a variation of 30% between the highest and lowest value, which can be explained by the pores and non-homogeneity of the material. Kazamer et al., in a study evaluating a similar alloy applied by Flame Spraying on low-alloy steel,

found a maximum hardness of 890 HV_{0.3} with 30% variation for the as sprayed coating without remelting [32].

3.2. Creep Test

Table 4 presents the results obtained in the creep tests at 550 °C, equivalent to 0.36 of the melting temperature of AISI 4340 steel (1427 °C), with stresses of 200, 250, and 300 MPa. The primary time (t_p), the secondary creep rate (ϵ_s), the final creep time (t_f), and the final strain (ϵ_f) are detailed.

Table 4. Results of creep tests at 550 °C.

| s (MPa) | Condition | t_p (h) | ϵ_s (1/h) | t_f (h) | ϵ_f (mm/mm) |
|---------|-----------|-----------|------------------------|-----------|----------------------|
| 200 | Pristine | 10.01 | 5.264×10^{-5} | 144.77 | 0.016 |
| 250 | | 8.00 | 0.521×10^{-4} | 65.98 | 0.009 |
| 300 | | 2.00 | 3.645×10^{-4} | 13.47 | 0.010 |
| 200 | Coated | 10.01 | 1.315×10^{-5} | 187.23 | 0.0157 |
| 250 | | 3.21 | 1.206×10^{-4} | 50.44 | 0.015 |
| 300 | | 1.00 | 5.354×10^{-4} | 12.93 | 0.018 |

The secondary creep rate decreased for the coated sample at a load of 200 MPa, which indicates an increase in creep resistance at this temperature and load. The time to fracture in this condition was longer. At the lower test load the presence of the coating inhibits substrate deformation in tension, accommodating stresses at this loading level, reducing the cross-sectional stress and avoiding oxidation of the substrate during long time creep. There was no spalling or cracking of the coating on the gauge section of the tested sample prior to the final narrowing caused by the deformation of the underlying material. According to previous works, the coated samples have presented a better behavior in creep tests for coated or treated samples at low loads from 70 to 230 MPa [12–14]. In such circumstances, both the coating and steel substrate can be considered as a composite system that sustains the entire creep load during the testing phase, which has been confirmed by other authors [13,14]. According to the research of Zhang et al. [14], the coating's presence generates a division in the applied load between the coating and substrate, decreasing the load that the substrate endures. Under higher loading conditions of 250 and 300 MPa, the secondary creep rate increased for the coated sample. The time to fracture decreases for the load of 250 MPa and 300 MPa. This result can be attributed to oxides, leaving the coating layer brittle and subject to fracture at higher loads. It can be also concluded that the increase in creep rate for higher test loads is caused by early failure of the coating then transferring all the load to the substrate. The atmospheric plasma coating process generally presents oxidation of the coating in two stages, during the flight of the particles in the spray and at the moment of impact on the substrate [33]. Experimental results have shown that the Ni-based coating has a low tendency to oxidize during the spraying process but tends to oxidize after impacting the substrate [34]. Since only one sample was tested for each condition, no definitive statement can be made from this study. The tendencies observed here require further confirmation.

The creep curves obtained at 550 °C and 200, 250, and 300 MPa, corresponding to the deformation as a function of time, are shown in Figures 6–8 for conditions with and without coating. It is possible to observe in the analysis of the creep curves that, even in the tensions of 250 and 300 MPa, the deformations are minor for the samples coated in the first hours of the test, while this trend inverted with the passage of the loading time.

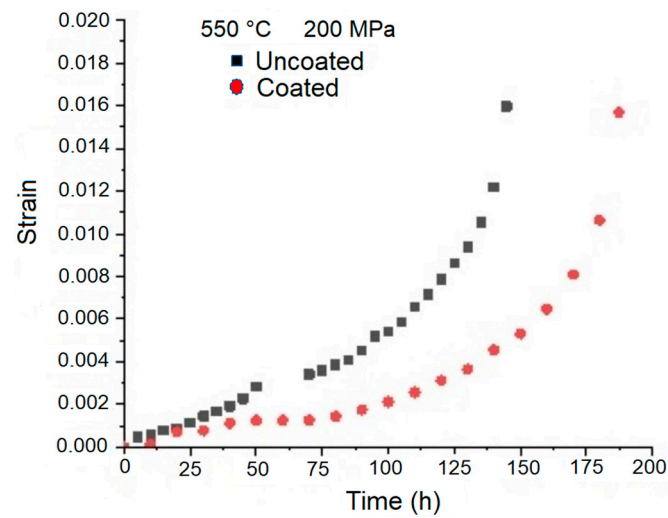


Figure 6. Creep curves at 550 °C/200 MPa.

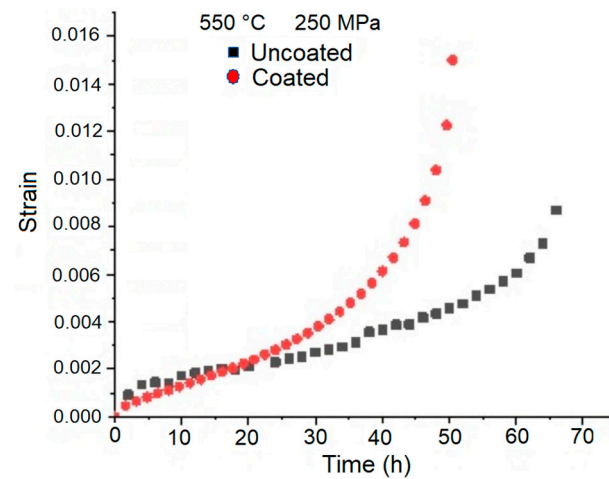


Figure 7. Creep curves at 550 °C/250 MPa.

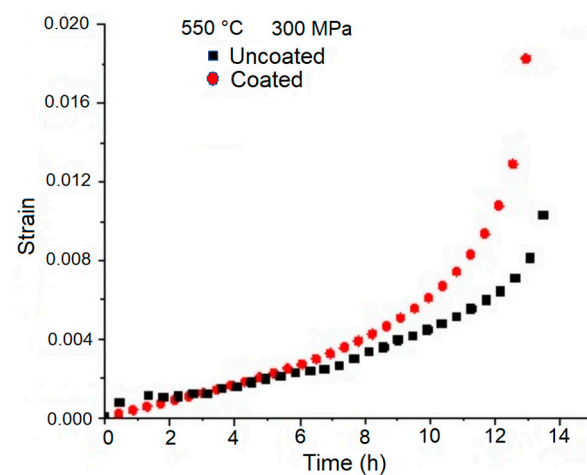


Figure 8. Creep curves at 550 °C/300 MPa.

3.3. Fractographic Analysis

The fractography images of the creep tested samples are shown in Figure 9 for the uncoated samples, and in Figures 10–12 for the coated samples at different loads. In all samples, it is possible to observe the presence of microcavities, pointing to an intergranular ductile fracture as defined by Evans and Wilshire [35]. Under high temperatures,

microfractures occurred along the grain boundary in an intergranular manner as in the case of those identified by Zhao et al. working with welded joints (cc) [36]. External stress can cause grain boundary sliding, leading to crack initiation and deformation of the specimen leading to failure. The results agree with the morphology of the fracture surface defined in the work of Ranieri that assess the behavior of plasma nitrided 4340 Steel [37]. In plasma nitrocarburizing coating work on AISI 4340 steel, performed by Li et al., the creep failure morphology had similar aspects, with microcavities and ductile fracture, both in coated and uncoated conditions [38]. The coated specimens show good adhesion to almost the entire perimeter of the sample under conditions of 200 and 250 MPa, with partial detachment in some areas. At 300 MPa, detachment occurred around the entire perimeter in the fracture region. The coating layer shown in Figure 11c reveals characteristic deposition for this type of coating [39]. The predominant mechanism in these tests were the formation and coalescence of microcavities [40].

For the coated specimens subjected to loads of 250 and 300 MPa, the creep rate and the final rupture time were found to be lower than those of the uncoated sample, as indicated in Table 3. Residual stresses may have arisen on the coating due to the rapid cooling process during atmospheric plasma deposition [41]. These stresses are crucial in atmospheric plasma coatings, as they can cause coating deformations or the formation of cracks [42].

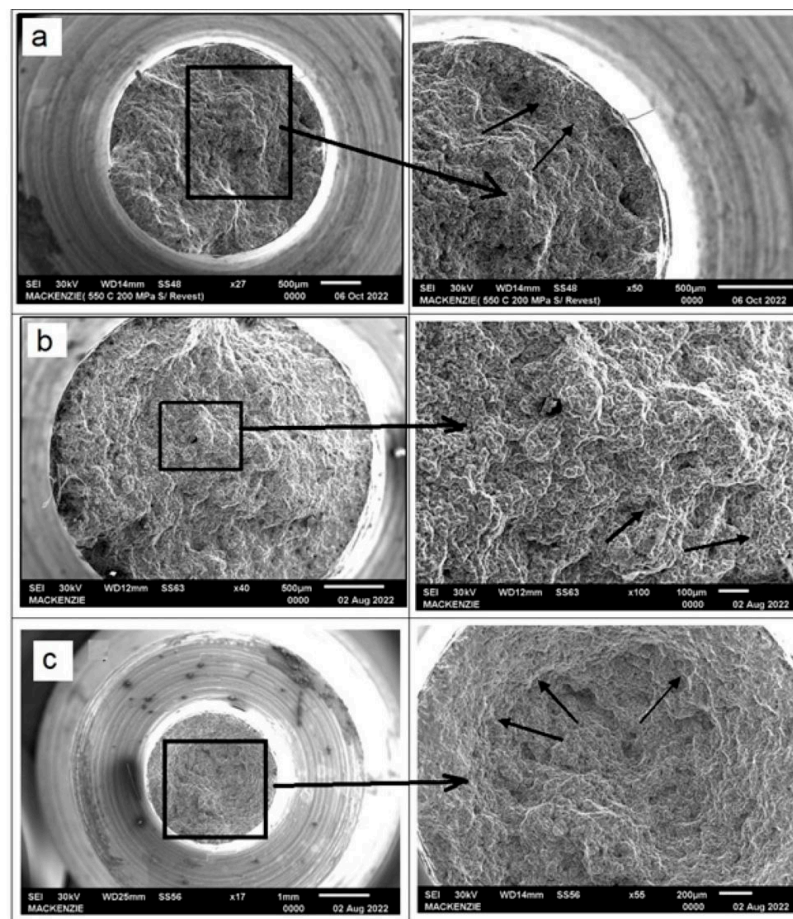


Figure 9. Images of the fracture surface of the uncoated specimen at 550 °C with the stress of (a) 200 MPa, (b) 250 MPa, and (c) 300 MPa.

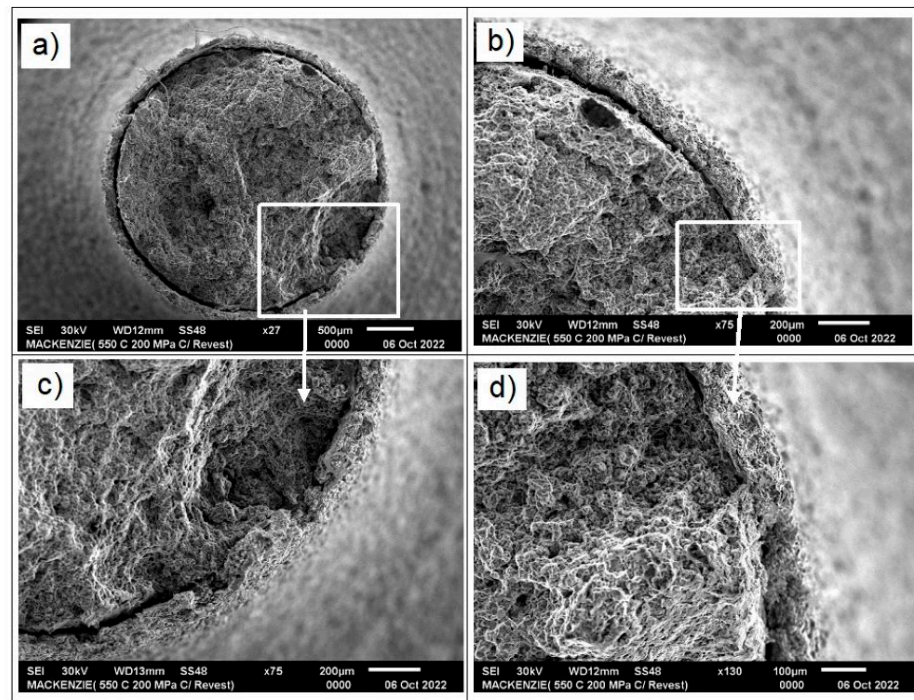


Figure 10. The fracture surface of the coated sample at 550 °C and 200 MPa: (a) full section, (b) enlargement of the upper right side, (c) detail of the partial coating detachment, (d) detail of the adhered coating.

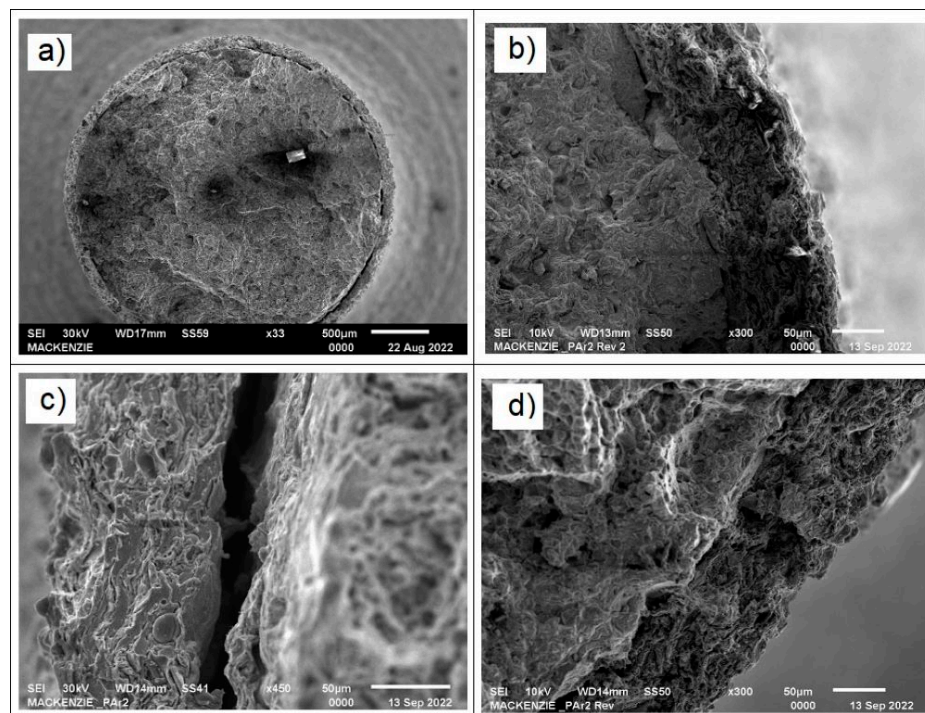


Figure 11. The fracture surface of the coated sample at 550 °C and 250 MPa: (a) full section, (b) enlargement of the upper right side, (c) detail of the partial coating detachment, (d) detail of the full adhered coating.

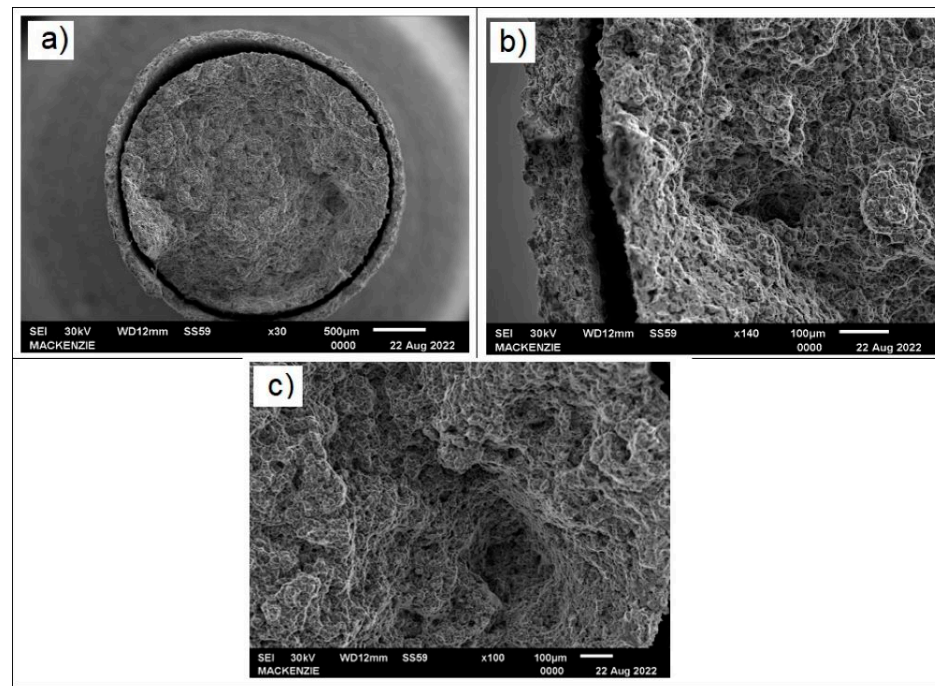


Figure 12. The fracture the surface of the coated sample at 550 °C and 300 MPa: (a) full section with completely detached coating, (b) enlargement of the left side, (c) detail of the coating characteristic microstructure.

Figure 13 shows the sequence of micrographs of the sample tested at 300 MPa, where the most extensive coating detachment occurred from the crack region (a) to approximately the middle of the sample (d). It is possible to observe that the separation of the coating around the crack is not observed throughout the entire specimen, concentrating on the portion closest to the crack. One can also clearly see several fractures in the coating, which can reduce coating resistance and lead to a decrease in the creep rate [43].

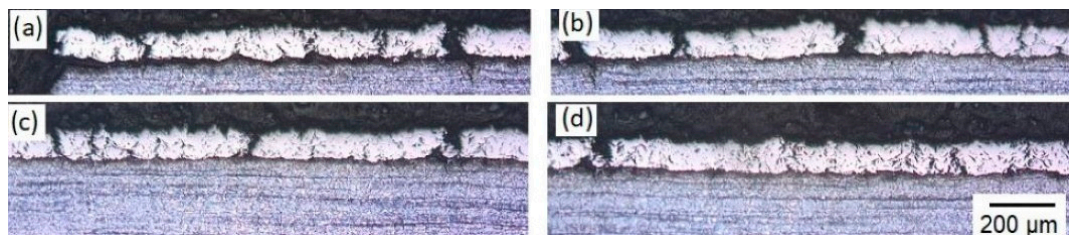


Figure 13. Optical longitudinal cross section images of the coated sample at 550 °C and 300 MPa showing the adhesion of the coating to the substrate and some fractures of the coating at (a) left side, (b) center-left, (c) center-right, (d) right side.

Figure 14 shows an intermediate oxide layer between the coating and substrate. This thick oxide layer can be seen along the entire coating/substrate interface. As the oxide layer between the substrate and the coating prior to the creep test was very thin, it can be concluded that an oxide layer of 10 to 15 µm formed during the test due to the high temperature. In the APS process, oxidation is typically divided into two stages: oxidation during particle flight and upon impact with the substrate. It is known that the amount of Si, B and C affects oxidation in the APS process, and that oxidation after impact is superior to oxidation during particle flight. The formation of the oxide layer is affected by environmental and temperature conditions, and the microstructure of the coating. This leads to the formation of a continuous layer between the substrate and the coating. The initial oxide layer that was identified from the coating was very thin, around 2 µm.

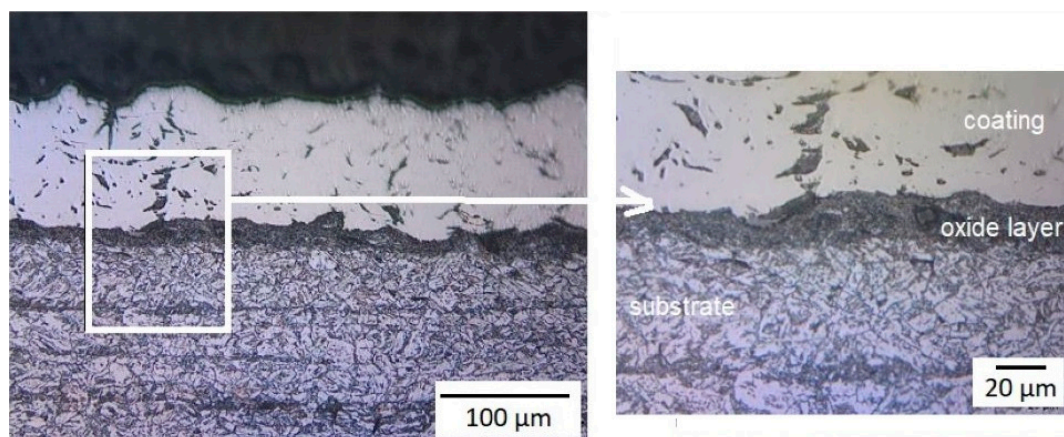


Figure 14. Cross sectional longitudinal optical images of the tested sample with the oxide layer formed on the substrate.

This study has some limitations that prevent further conclusions from being drawn. These limitations are the reduced number of tested samples, the influence of the increased test temperature, and variations in the coating thickness. Further investigations are required to determine the reason behind the failure of the coated samples at loads exceeding 200 MPa at this particular test temperature. Currently, creep tests are being developed at the same loads but at higher temperatures, which will aid in comprehending the impact of the coating on the creep behavior of AISI 4340 steel. X-ray diffraction is scheduled to be conducted to determine the phase content and influence of any possible phase formations.

4. Conclusions

The following are the main conclusions that can be drawn from this study

- The samples coated with a nickel-based self-fluxing alloy promoted an increase in the final rupture time during creep and a decrease in the creep rate in stage II (stationary) under the stress load of 200 MPa.
- At loads of 250 and 300 MPa, the creep rate was higher for the coated sample.
- At loads higher than 200 MPa the effect of the coating is harmful to the substrate at tensile creeping by initiating the crack nucleation and further propagation.
- Crack propagation showed a ductile behaviour, leading to failure due to mechanical overload, in line with work carried out with this type of steel.
- The detachment of the coating in the crack region occurred due to mechanical overload, mainly at loads higher than 300 MPa.
- The oxide layer formed between the coating and the substrate can cause a decrease in adhesion, resulting in lower creep resistance at higher stresses.

Author Contributions: Conceptualization, D.A.M. and C.R.C.L.; methodology, D.A.M. and G.F.C.A.; validation, A.A.C., C.R.C.L. and F.R.C.; investigation, D.A.M.; resources, G.F.C.A., F.R.C. and M.M.; writing—original draft preparation, D.A.M.; writing—review and editing, A.A.C. and C.R.C.L.; supervision, A.A.C. and C.R.C.L.; project administration, C.R.C.L.; funding acquisition, M.M. All authors have read and agreed to the published version of the manuscript.

Funding: This research received no external funding.

Institutional Review Board Statement: Not applicable.

Informed Consent Statement: Not applicable.

Data Availability Statement: The data presented in this study are available on request from the corresponding author. The data are not publicly available because is waiting for the registration in the Mackenzie repository.

Acknowledgments: The authors express their gratitude for the organizational support provided by the CAPES-PRINT Program. D. Moraes acknowledges Mackenzie Presbyterian University for the support during the project development.

Conflicts of Interest: The authors declare no conflict of interest.

References

1. Roy, S.; Kumar, R.; Das, R.K.; Sahoo, A.K. A Comprehensive Review on Machinability Aspects in Hard Turning of AISI 4340 Steel. *IOP Conf. Ser. Mater. Sci. Eng.* **2018**, *390*, 012009. [\[CrossRef\]](#)
2. Mehrabi, A.; Sharifi, H.; Asadabad, M.A.; CorrectedNajafabadi, R.A.; Rajaei, A. Improvement of AISI 4340 steel properties by intermediate quenching-microstructure, mechanical properties, and fractography. *Int. J. Mat. Res.* **2020**, *111*, 9. [\[CrossRef\]](#)
3. Lee, W.S.; Su, T.T. Mechanical properties and microstructural features of AISI 4340 high-strength alloy steel under quenched and tempered conditions. *J. Mater. Process. Technol.* **1999**, *87*, 198–206. [\[CrossRef\]](#)
4. Nunes, M.M.; Silva, E.M.D.; Renzetti, R.A.; Brito, T.G. Analysis of Quenching Parameters in AISI 4340 Steel by Using Design of Experiments. *Mater. Res.* **2018**, *22*, e20180315. [\[CrossRef\]](#)
5. Sklenicka, V.; Kral, P.; Dvorak, J.; Takizawa, Y.; Masuda, T.; Horita, Z.; Kucharova, K.; Kvapilova, M.; Svobodova, M. Effects of Grain Refinement and Predeformation Impact by Severe Plastic Deformation on Creep in P92 Martensitic Steel. *Adv. Eng. Mater.* **2019**, *22*, 1900448. [\[CrossRef\]](#)
6. Lehmusto, J.; Yrjas, P.; Hupa, L. Pre-oxidation as a means to increase corrosion resistance of commercial superheater steels. *Oxid. Met.* **2019**, *91*, 311. [\[CrossRef\]](#)
7. Karimbaev, R.; Pyun, Y.S.; Maleki, E.; Unal, O.; Amanov, A. An improvement in fatigue behavior of AISI 4340 steel by shot peening and ultrasonic nanocrystal surface modification. *Mater. Sci. Eng. A* **2020**, *791*, 139752. [\[CrossRef\]](#)
8. Hou, X.; Zhang, H.; Seraffon, M.; Fry, A.T. Steam oxidation and mechanical performance of a ferritic–martensitic steel with slurry aluminide coating. *Mater. Corros.* **2020**, *71*, 1310–1320. [\[CrossRef\]](#)
9. Dryepontd, S.; Zhang, Y.; Pint, B.A. Creep and corrosion testing of aluminide coatings on ferritic–martensitic substrates. *Surf. Coat. Technol.* **2006**, *201*, 3880–3884. [\[CrossRef\]](#)
10. Chang, J.-K.; Lin, C.-S.; Wang, W.-R.; Jian, S.-Y. High temperature deformation behaviors of hot dip 55 wt% Al-Zn coated steel. *Appl. Surf. Sci.* **2020**, *511*, 145550. [\[CrossRef\]](#)
11. Parekh, T.; Patel, P.; Sasmal, C.S.; Jamnapara, N.I. Effect of plasma processed Ti-Al coating on oxidation and tensile behavior of Ti6Al4V alloy. *Surf. Coat. Technol.* **2020**, *394*, 125704. [\[CrossRef\]](#)
12. Bates, B.L.; Zhang, Y.; Dryepontd, S.; Pint, B.A. Creep behavior of pack cementation aluminide coatings on Grade 91 ferritic–martensitic alloy. *Surf. Coat. Technol.* **2013**, *240*, 32–39. [\[CrossRef\]](#)
13. Zhang, X.C.; Liu, C.J.; Xuan, F.Z.; Wang, Z.D.; Tu, S.T. Effect of NiCr and NiCrAl coatings on the creep resistance of a Ni alloy. *Mater. Sci. Eng. A* **2011**, *528*, 2282–2287. [\[CrossRef\]](#)
14. Zhang, X.Z.; Wu, X.J.; Liu, R.; Yao, M.X. Effects of oxidation-resistant coating on creep behavior of modified 9Cr-1Mo steels. *Mater. Sci. Eng. A* **2019**, *743*, 418–424. [\[CrossRef\]](#)
15. Xu, Y.; Yang, X.; Lu, J.; Huang, J.; Li, W. Mechanism of accelerating creep rupture under high stress level of pack cementation aluminide coatings deposited onto T92 steel tube. *Surf. Coat. Technol.* **2023**, *455*, 129212. [\[CrossRef\]](#)
16. Simunovic, K.; Havrlisan, S.; Saric, T.; Vukelic, D. Modeling and Optimization in Investigating Thermally Sprayed Ni-Based Self-Fluxing Alloy Coatings: A Review. *Materials* **2020**, *13*, 4584. [\[CrossRef\]](#)
17. Mrdak, M.; Vencl, A.; Čosić, M. Microstructure and Mechanical Properties of the Mo-NiCrBSi Coating Deposited by Atmospheric Plasma Spraying. *FME Trans.* **2009**, *37*, 27–32.
18. Simunovic, K.; Saric, T.; Simunovic, G. Different Approaches to the Investigation and Testing of the Ni-Based Self-Fluxing Alloy Coatings-A Review. Part 1: General Facts, Wear and Corrosion Investigations. *Tribol. Trans.* **2014**, *57*, 955. [\[CrossRef\]](#)
19. Gan, J.A.; Berndt, C.C. Review on the Oxidation of Metallic Thermal Sprayed Coatings: A Case Study with Reference to Rare-Earth Permanent Magnetic Coatings. *J. Therm. Spray Technol.* **2013**, *22*, 1069–1091. [\[CrossRef\]](#)
20. Davis, J.R. *Handbook of Thermal Spray Technology*; ASM International: Material Park, OH, USA, 2004.
21. Lorenzo-Bañuelos, M.; Díaz, A.; Rodríguez, D.; Cuesta, I.; Fernández, A.; Alegre, J. Influence of Atmospheric Plasma Spray Parameters (APS) on the Mechanical Properties of Ni-Al Coatings on Aluminum Alloy Substrate. *Metals* **2021**, *11*, 612. [\[CrossRef\]](#)
22. Li, C.J.; Luo, X.T.; Dong, X.Y.; Zhang, L.; Li, C.X. Recent Research Advances in Plasma Spraying of Bulk-Like Dense Metal Coatings with Metallurgically Bonded Lamellae. *J. Therm. Spray Technol.* **2022**, *31*, 5–27. [\[CrossRef\]](#)
23. Miguel, J.R.; Guilemany, J.M.; Vizcaino, S. Tribological study of NiCrBSi coating obtained by different processes. *Tribol. Int.* **2003**, *36*, 181–187. [\[CrossRef\]](#)
24. Holdsworth, S. Creep-Fatigue Failure Diagnosis. *Materials* **2015**, *8*, 7757–7769. [\[CrossRef\]](#) [\[PubMed\]](#)
25. Onck, P. Growth of an initially sharp crack by grain boundary cavitation. *J. Mech. Phys. Solids* **1999**, *47*, 99–139. [\[CrossRef\]](#)
26. *ASTM E139-11*; Standard Test Methods for Conducting Creep, Creep Rupture, and Stress Rupture Tests of Metallic Materials. ASTM: West Conshohocken, PA, USA, 2011; p. 11.
27. *ASTM A29/A29M*; Standard Specifications for General Requirements for Steel Bars, Carbon and Alloy, Hot-Wrought. ASTM International: West Conshohocken, PA, USA, 2013.

28. DSMTS-0026.7; Oerlikon Metco: Pfäffikon, Switzerland, 2016. Available online: <http://successcompass.com.sa/wp-content/uploads/2016/12/Oerlikon-Metco-Materials-Guide.pdf> (accessed on 25 August 2020).
29. Mellali, M.; Grimaud, A.; Leger, A.C.; Fauchais, P.; Lu, J. Alumina grit blasting parameters for surface preparation in the plasma spraying operation. *J. Therm. Spray Technol.* **1997**, *6*, 217–227. [[CrossRef](#)]
30. Yang, J.; Qu, K.; Yang, J. Fatigue performance of Q355B steel substrate treated by grit blasting with and without subsequent cold spraying with Al and Cu. *Surf. Coat. Technol.* **2021**, *405*, 126662. [[CrossRef](#)]
31. Barros, R.A.; Abdalla, A.J.; Rodrigues, H.L.; Pereira, M.D.S. Caracterização de um aço AISI/SAE 4340 com diferentes microestruturas através da técnica de triplíce ataque. *Rev. Bras. Aplic. Vácuo.* **2015**, *34*, 71–74. [[CrossRef](#)]
32. Kazamer, N.; Muntean, R.; Vălean, P.C.; Pascal, D.T.; Mărginean, G.; Șerban, V.A. Comparison of Ni-Based Self-Fluxing Remelted Coatings for Wear and Corrosion Applications. *Materials* **2021**, *14*, 3293. [[CrossRef](#)]
33. Zeng, Z.; Kuroda, S.; Era, H. Comparison of oxidation behaviour Ni-20Cr alloy and Ni-based self-fluxing alloy during air plasma spraying. *Surf. Coat. Technol.* **2009**, *204*, 69–77. [[CrossRef](#)]
34. Lee, J.S.; Armaki, H.G.; Maruyama, K.; Muraki, T.; Asahi, H. Causes of breakdown of creep strength in 9Cr–1.8W–0.5Mo–VNB steel. *Mater. Sci. Eng. A-Struct.* **2006**, *428*, 270. [[CrossRef](#)]
35. Evans, R.W.; Wilshire, B. *Introduction to Creep*; Oakdale Printing Company: London, UK, 1993.
36. Zhao, L.; Jing, H.; Xiu, J.; Han, Y.; Xu, L. Experimental investigation of specimen size effect on creep crack growth behavior in P92 steel welded joint. *Mater. Des.* **2014**, *57*, 736. [[CrossRef](#)]
37. Ranieri, A. Caracterização Mecânica e Microestrutura de em aço 4340 em Estruturas Multifásicas e Pratinamento de Nitrocarbônica a Plasma. Ph.D. Thesis, UNESP, Guaratinguetá, Brazil, 2010.
38. Li, Y.F.; Wang, L.; Zhang, G.; Qi, D.Q.; Du, K.; Lou, L.H. Anisotropic Stress Rupture Properties of a 3rd-Generation Nickel-Based Single-Crystal Superalloy at 1100 °C/150 MPa. *Acta Metall. Sin.* **2020**, *33*, 446. [[CrossRef](#)]
39. Higuera, V.; Belzunce, F.J.; Carriles, A.; Poveda, S. Influence of the thermal-spray procedure on the properties of a nickel-chromium coating. *J. Mater. Sci.* **2002**, *37*, 649–654. [[CrossRef](#)]
40. Waki, H.; Ogura, K.; Nishikawa, I.; Kashihara, Y. Residual Stress Measurement of Plasma-Sprayed Coatings. *JSME Int. J. A-Solid M* **2003**, *46*, 590–597. [[CrossRef](#)]
41. Kuroda, S.; Clyne, T.W. The quenching stress in thermally sprayed coatings. *Thin Solid Films* **1991**, *200*, 49–66. [[CrossRef](#)]
42. Xuan, F.Z.; Chen, J.J.; Wang, Z.; Tu, S.T. Time-dependent deformation and fracture of multi-material systems at high temperature. *Int. J. Press. Vessel. Pip.* **2009**, *86*, 604–615. [[CrossRef](#)]
43. Pershin, V.; Lufitha, M.; Chandra, S.; Mostaghimi, J. Effect of Substrate Temperature on Adhesion Strength of Plasma-Sprayed Nickel Coatings. *J. Therm. Spray Technol.* **2003**, *12*, 370–376. [[CrossRef](#)]

Disclaimer/Publisher’s Note: The statements, opinions and data contained in all publications are solely those of the individual author(s) and contributor(s) and not of MDPI and/or the editor(s). MDPI and/or the editor(s) disclaim responsibility for any injury to people or property resulting from any ideas, methods, instructions or products referred to in the content.